HHS Public Access

Author manuscript

Biol Psychiatry. Author manuscript; available in PMC 2024 August 15.

Published in final edited form as:

Biol Psychiatry. 2023 August 15; 94(4): 297–309. doi:10.1016/j.biopsych.2023.03.020.

GluN2D subunit in parvalbumin interneurons regulates prefrontal cortex feed-forward inhibitory circuit and molecular networks relevant to schizophrenia

Dinesh Y. Gawande[1,*], **Kishore Kumar S. Narasimhan**[1,#,*], **Gajanan P. Shelkar**[1], **Ratnamala Pavuluri**[1], **Holly A. F. Stessman**[1], **Shashank M. Dravid**[1,#]

[1]Department of Pharmacology and Neuroscience, Creighton University School of Medicine, Omaha NE 68178

Abstract

Background: Parvalbumin interneuron (PVI) activity synchronizes medial prefrontal cortex (mPFC) circuit for normal cognitive function and its impairment may contribute to schizophrenia (SZ). NMDA receptors in PVIs participate in these activities and form the basis for NMDA receptor hypofunction hypothesis of SZ. However, the role of GluN2D subunit, enriched in PVIs, in regulating molecular networks relevant to SZ is unknown.

Methods: Using electrophysiology and mouse model with conditional deletion of GluN2D from PVIs (PV-GluN2D KO) we examined the cell excitability and neurotransmission in mPFC. Histochemical, RNAseq analysis and immunoblotting were conducted to understand molecular mechanisms. Behavioral analysis was conducted to test cognitive function.

Results: PVIs in mPFC were found to express putative GluN1/2B/2D receptors. In PV-GluN2D KO model PVIs were hypoexcitable whereas pyramidal neurons were hyperexcitable. Excitatory neurotransmission was higher in both cell types in PV-GluN2D KO whereas inhibitory neurotransmission showed contrasting changes which could be explained by reduced somatostatin interneuron projections and increased PVI projections. Genes associated with GABA synthesis,

[#]Corresponding Authors: 1) Dr. Shashank M. Dravid, Department of Pharmacology and Neuroscience, Creighton University, School of Medicine, 2500 California Plaza, Omaha, NE 68178, Phone: 402-280-1885, Fax: 402-280-2142, ShashankDravid@creighton.edu, 2) Dr. Kishore Kumar S. Narasimhan, Department of Pharmacology and Neuroscience, Creighton University, School of Medicine, 2500 California Plaza, Omaha, NE 68178, Phone: 402-280-5004, KishoreKumarsNarasimhan1@creighton.edu.

[*]Equal contribution

Author contributions:
Conceptualization: DYG, KKSN, GPS, SMD
Methodology: DYG, KKSN, GPS, HAFS, SMD
Investigation: DYG, KKSN, GPS, RP, HAFS, SMD
Visualization: DYG, KKSN, GPS, RP, HAFS, SMD
Supervision: SMD
Original draft composition, review & editing: DYG, KKSN, GPS, SMD

Ethics approval: All animal studies were approved by Creighton University, Institutional Animal Care and Use Committee.

Data and materials availability: All data needed to evaluate the conclusions in the paper are present in the paper and/or the Supplementary Materials. Data is available from the corresponding author upon reasonable request.

Conflict of interest: The authors report no biomedical financial interests or potential conflicts of interest.

vesicular release, and uptake as well as those involved in formation of inhibitory synapses specifically GluD1-Cbln4 and Nlgn2 and regulation of dopamine terminals were downregulated in PV-GluN2D KO. SZ-susceptibility genes including Disc1, Nrg1 and ErbB4 and their downstream targets were also downregulated. Behaviorally PV-GluN2D KO mice showed hyperactivity and anxiety behavior and deficits in short-term memory and cognitive flexibility.

Conclusion: These findings demonstrate that GluN2D in PVIs serve as a point of convergence of pathways involved in the regulation of GABAergic synapses and relevant to SZ.

Keywords

GluN2D; GABAergic; mPFC; Nrg1-ErbB4 signaling; parvalbumin; schizophrenia

Introduction

Parvalbumin-expressing GABAergic neurons play an important role in regulating local circuits. Synchronous recruitment of parvalbumin interneurons (PVIs) in the medial prefrontal cortex (mPFC) generates gamma oscillation rhythms that emerge in the performance of cognitive tasks. A deficit in inhibitory neurotransmission via PVIs has been observed in several neuropsychiatric disorders including schizophrenia (SZ) [1–3], where downregulation of the PV and GAD67 proteins is consistently observed [4–11] and may underlie disruption in synchrony between brain regions and cognitive and negative symptoms of the disease [12–14].

NMDA receptors contribute significantly to the function of interneurons. Converging studies using genetic models, with conditional ablation of the obligatory NMDA receptor GluN1 subunit, have demonstrated that early developmental reduction in NMDA receptor activity in GABAergic interneurons particularly PVIs leads to emergence of behavioral, cognitive and gamma oscillation deficits [15–18]. These findings are consistent with the NMDA receptor hypofunction hypothesis of SZ which is further supported by genetic, biochemical and pharmacological studies [1, 19–22]. However, a limitation of these studies is that they do not address the subtype specific role of NMDA receptor in SZ. In addition, the effect of NMDAR receptor dysfunction in PVIs on circuits and downstream pathways is not well understood.

NMDA receptors are tetrameric complexes composed of two GluN1 and two GluN2 subunits. The GluN2 subunit subtypes (GluN2A-GluN2D) confer distinct physiological and pharmacological properties to the receptor complex. While GluN2A/2B are widely expressed throughout the brain, GluN2C/2D subunit has unique expression patterns. In the cortico-limbic regions, GluN2C is expressed in astrocytes [23, 24], whereas GluN2D subunits are enriched in interneurons including PV-positive [25–27]. GluN2D-containing receptors display properties such as slow deactivation, lack of desensitization, low sensitivity to Mg^{2+}-block and high agonist affinity [28, 29] ideal for tonic activity, which may support cortical oscillations [30, 31]. Finally, mutations and polymorphisms associated with SZ, developmental delay and infantile epilepsy have been found in GRIN2D gene, which codes for GluN2D, further supporting its relationship to circuit dysfunction [32, 33]. Using a novel conditional PVI specific GluN2D KO model, here we directly examined the role of GluN2D

subunit in the PVIs in regulating mPFC circuit. To address this, we analyzed the molecular networks through transcriptomics and performed electrophysiological and behavioral studies to determine the excitatory-inhibitory balance and cognitive function, respectively. Our results demonstrate that GluN2D ablation from PVIs results in mPFC hyperexcitation and impaired feed-forward inhibitory circuit and changes in genes critical for GABAergic as well as dopaminergic synapse function and genes that are highly associated with SZ, thus providing novel insights into the NMDA receptor hypofunction in SZ.

Material and Methods

Details of the methods are included in supplementary information. Conditional deletion of GluN2D from PVIs was achieved by crossing PV-Cre mouse line with GluN2D$^{flox/flox}$ mice as previously described [34]. Electrophysiology, molecular and behavioral studies were performed on age matched male and female mice. No significant differences were observed when comparing genotypes based on sexes and therefore male and female data were pooled (additional information in supplementary methods). All procedures were approved by the Creighton University IACUC. For electrophysiological recordings in acute brain slices, 300 μm thick coronal slices were prepared. A picospritzer was used to evoke puff-induced currents. For whole-cell current-clamp recordings, hyper- and de-polarizing current steps were applied for 500 ms in 40-pA increments from −400 pA to 400 pA. For spontaneous excitatory postsynaptic currents (sEPSC) and spontaneous inhibitory postsynaptic currents (sIPSC) voltage-clamp recordings were performed at −70 mV and 0 mV holding potential respectively. For mRNA collection and RNAseq analysis, samples were prepared using RNAeasy kit and library preparation and sequencing was outsourced to Novogene. Behavioral tests were conducted in male and female mice to assess behaviors relevant to SZ phenotypes including cognitive function as previously described [35–37]. Statistical analyses were performed using Prism 7 (GraphPad Software).

Results

PV interneurons express NMDA receptors with GluN1/2B/2D stoichiometry

We have recently developed a conditional knockout mouse for selective ablation of GluN2D from PVIs by crossing PV-Cre with GluN2D$^{flox/flox}$ mice [34]. The GluN2D$^{flox/flox}$ mice were generated by removing the reporter cassette by crossing Grin2D$^{tm1a(EUCOMM)Wtsi}$ mice from Wellcome Trust Sanger Institute using B6-SJL-Tg(ACTFLPe)9205Dym/J line. Using electrophysiology, we examined the subunit composition and GluN2D contribution to NMDARs in PVIs in the mPFC and the effect of PV-CreGluD1$^{flox/flox}$ (PV-GluN2D KO). NMDA receptor responses were elicited by puff application of agonists onto labeled PVIs in the mPFC of PV-Cre WT mice (Figure 1B) and the effect of GluN2C/2D inhibitor DQP1105 was evaluated. DQP1105 reduced the amplitude of NMDA receptor responses by ~40% (Figure 1C–C’), consistent with effects of GluN2C/2D inhibitor/potentiator in in previous studies [25, 38, 39]. The decay kinetics under control and DQP1105 conditions were not significantly different (data not shown), suggesting that GluN2D subunit potentially forms triheteromeric receptors with other GluN2 subtypes instead of forming independent diheteromeric receptors. Furthermore, a significant reduction in currents was

observed by GluN2B-selective antagonist Ro-25–6981 applied with DQP1105, however only a modest additional reduction in currents was observed by GluN2A-selective antagonist TCN201. Finally, glutamate-site competitive antagonist AP5 inhibited the remaining currents demonstrating these were GluN2-dependent NMDA receptor currents. Together, these results demonstrate that PVIs in the mPFC primarily express NMDA receptors with a putative triheteromeric GluN1/GluN2B/GluN2D stoichiometry.

We next assessed the effect of conditional ablation of GluN2D from PVIs on NMDA receptor responses in mPFC. The GluN2C/2D inhibitor DQP1105 did not inhibit NMDA receptor currents from PVIs in PV-GluN2D KO mice, demonstrating loss of contribution of GluN2D subunit (Figure 1C–C'). Ro-25–6981 produced a robust reduction in the amplitude of NMDA receptor responses in PV-GluN2D KO mice and TCN201 also significantly reduced the NMDA receptor responses. Together, these results suggest that upon loss of GluN2D from PVIs, the subunit composition is putatively GluN1/GluN2A/GluN2B. No significant change in the overall amplitude of the puff-induced responses were observed in PV-GluN2D KO (PV-Cre = 181.5 ± 23.8 pA and PV-GluN2D KO = 208.4 ± 28.4 pA), suggesting primarily a shift in the subunit composition. In western blotting analysis a significant reduction in the expression of GluN2D was observed in PV-GluN2D KO (Figure 1D).

Conditional ablation of GluN2D leads to higher excitatory neurotransmission onto PV interneurons in the mPFC

We next evaluated the effect of deletion of GluN2D on PVI function in the mPFC. In current-clamp recordings, we first examined the excitability of PVIs when the membrane potential was normalized to −65 mV. Under these conditions we found that the PVI spike frequency was significantly reduced in PV-GluN2D KO mice (Figure 1F). No change in action potential half-width was observed but the inter-event-interval was significantly higher in PV-GluN2D KO (Figure 1F, G). Interestingly at resting membrane potential, no change in spike frequency was observed between the genotypes (Figure 1H). No change in resting membrane potential was observed in PV-GluN2D KO (Figure 1I) suggesting that difference in excitability were not due to shift in resting membrane potential. Moreover, these results suggest potential homeostatic mechanisms in PVIs of PV-GluN2D KO to normalize excitability under resting conditions. A significant increase in cell capacitance was observed (PV-Cre = 31.09 ± 1.28 pF vs PV-GluN2D KO = 38.08 ± 2.27 pF, $p = 0.016$, N = 11–12) which may partially account for change in cell excitability. No change in cell body size (data not shown) or after hyperpolarization (PV-Cre = −7.14 ± 1.58 mV vs PV-GluN2D KO = −8.93 ± 1.22 mV) was found. In addition, RNAseq data presented later suggested no change in expression of voltage-gated sodium channel. It is possible that functional changes in voltage-gated channels may also underlie differences in excitability. We next assessed excitatory neurotransmission in PVIs. In voltage-clamp recordings from labeled PVIs, we observed a significantly higher sEPSC frequency in PVIs of PV-GluN2D KO with no change in amplitude (Figure 1J) demonstrating increase in excitatory neurotransmission input onto PVIs.

Pyramidal neurons in PV-GluN2D KO are hyperexcitable and have higher excitatory neurotransmission

We next examined whether GluN2D function in PVIs affects excitability and excitatory neurotransmission of pyramidal neurons in the mPFC. In current clamp recordings with membrane potential normalized to −65 mV, we found a significantly higher spike frequency in response to stepwise current injection in pyramidal neurons in PV-GluN2D KO (Figure 2B). No change in half-width of action potential was observed but an increase in inter-event-interval was found (Figure 2C, D). At resting membrane potential, a similar increase in spike frequency of pyramidal neurons was observed (Figure 2E). Thus, unlike PVIs, pyramidal neurons showed hyperexcitability at both resting membrane potential as well as at −65 mV. No significant change was observed in resting membrane potential (Figure 2F) or cell capacitance (data not shown). Further a significant increase in the frequency of sEPSC was observed in PV-GluN2D KO (Figure 2G). No change in sEPSC amplitude was found. To test whether the increase in excitatory neurotransmission may involve changes in cortical versus thalamic inputs we conducted western blotting analysis for vGluT1 and vGluT2 which are markers for cortical and thalamic terminals respectively [40]. Interestingly, an increase in vGluT1 expression was observed in PV-GluN2D KO, whereas no change was seen in vGluT2 expression (Figure 2H). These results suggest primary change in cortico-cortical synaptic function in PV-GluN2D KO.

Altered feedforward inhibitory circuitry in the mPFC of PV-GluN2D KO

A large body of evidence have found altered GABAergic neurotransmission in models of neurodevelopmental disorders. Thus, we next assessed inhibitory neurotransmission in PVIs and pyramidal neurons. A significantly lower sIPSC frequency with no change in amplitude was observed in PVIs in PV-GluN2D KO (Figure 3A). In contrast, there was a significant increase in sIPSC frequency in layer 2/3 pyramidal neurons (Figure 3B). Similarly, an increase in inhibitory neurotransmission was observed in layer 5 pyramidal neurons (Figure S1). Previous studies suggest a feedforward circuitry in the mPFC where PVIs receive major inhibitory inputs from somatostatin (SST) neurons while pyramidal neurons receive stronger inhibitory inputs from PVIs [41]. Using immunohistochemistry, we examined changes in the projections of SST and PVIs. We found a significantly reduced SST puncta/elements in PV-GluN2D KO and a contrasting increase in PV puncta (Figure 3C, D). To test whether there are changes in inhibitory input from SST neurons or PVIs we conducted colocalization studies with the inhibitory synaptic marker GAD67. A significant reduction in the number of SST-GAD67 colocalized puncta (Figure 3E, F) and an increase in PV-GAD67 colocalized puncta was observed in PV-GluN2D KO (Figure 3G, C). Increase in PV was also observed in immunoblotting in PV-GluN2D KO (Figure S6). No change in total PVI cell number was observed in PV-GluN2D KO (PV Cre: 44.08 ± 1.003/10x field vs PV-GluN2D KO: 43.4 ± 1.392/10x field, $p = 0.6954$, n = 5 mice each). Overall, the increase in inhibitory neurotransmission in PVIs may results from a deficit in feed-forward inhibition from SST neurons together with an increase in PVI mediated GABAergic inputs onto pyramidal neurons.

Transcriptomic and enrichment analysis reveals changes in genes relevant to GABAergic neurotransmission and SZ upon ablation of GluN2D from PV interneurons

Next, we performed bulk RNAseq analysis on mPFC tissue to explore potential transcriptome changes and uncover molecular pathways involved in GluN2D function in PVIs. The analysis identified 196 differentially expressed genes (DEGs) between PV-Cre and PV-GluN2D KO, with 26 upregulated and 170 downregulated (Figure 4B). Figure 4D shows the heatmap comparison of DEGs. Gene set enrichment analysis (GSEA) including gene ontology (GO) biological processes were used to examine the upregulated and downregulated DEGs using Metascape [42]. The development of sensory organs, neuron migration, locomotory behavior, synapse signaling and organization, control of AMPA receptor activation and Wnt signaling, embryonic morphogenesis, and dopamine biosynthesis were among the processes that were downregulated (Figure S2). Synaptic enrichment analysis (SEA) of the DEGs using SynGo [43] indicated that the 47 genes among 196 identified DEGs were part of the synaptic biological processes, and 42 genes were part of the synaptic cellular components (Figure 4E). Thus, GluN2D deletion from PVIs leads to strong changes in synaptic signaling (Figure S2). Further disease enrichment analysis of the DEGs using Topp Gene suite [44] identified DEGs relevant to SZ, including Disc1, Nlgn2, Nrg1, ErbB4, Gad1 and Reln [45–52], as well as autism (Figure 4F).

To better understand the relevance of these genes to NMDA receptor hypofunction hypothesis we next evaluated the preferential cell-type expression of the DEGs by using the Drop Viz database [53]. Of the 196 DEGs, 81 genes were preferentially enriched in interneuron population (Figure 5A) including both the caudal ganglionic eminence (CGE; 51 genes) and medial ganglionic eminence (MGE; 30 genes) derived population (Figure 5B, C). In addition, 38 genes were enriched in neuronal subpopulations including claustrum Nr4a2, Layer5 Parm1, Layer5b Fezf2, and Layer6 Syt6. Further KEGG pathway analysis indicated the top five pathways including GABAergic synapses, calcium signaling, morphine addiction, extracellular matrix-receptor interaction, and renin secretion (Figure 5D, Figure S3–S5). Notably aberrant GABAergic synapse and calcium signaling upon GluN2D deletion in PVIs might be a contributing factor for SZ progression.

From the DEGs, we handpicked some of the targets to validate and determine whether the transcriptomic changes are reflected in the proteomic changes through western blot. We categorized these targets into “interneurons/GABAergic synapse”, “trans-synaptic molecules”, “dopaminergic synapse”, and “SZ relevant Nrg1-ErbB4 signaling”. First, consistent with transcriptomic analysis, we found a significant reduction in GAD67 and Calb2 whereas the expression of Gabra2 was elevated upon GluN2D deletion (Figure S6). Further, we determined the changes in trans-synaptic and synaptogenic proteins. Downregulation of Cbln1, Cbln4 and their synaptogenic partner GluD1 was observed in mPFC of PV-GluN2D KO (Figure 5E–F). Neuroligin-2 (Nlgn2), a postsynaptic cell-adhesion molecule of inhibitory synapses was also reduced in the PV-GluN2D KO mice (Figure 5E–F). Collectively, disrupted elements of GABAergic synapse and synaptogenic molecules confirm that there is an impaired inhibitory neurotransmission upon GluN2D deletion. Additionally, tyrosine hydroxylase (Th) relevant to dopaminergic synapse was also reduced (Figure 5E–F).

Next, we validated the mechanistic link between GluN2D deletion and changes SZ associated Nrg1-ErbB4 signaling, which is crucial in regulating excitatory–inhibitory (E–I) balance in the mPFC [54] and Akt-mTOR signaling. A significant reduction in both Nrg1 and ErbB4 was observed in PV-GluN2D KO mice (Figure 5G). Furthermore, the active forms (phosphorylated) of Akt and mTOR were significantly down in the mPFC of PV-GluN2D KO mice demonstrating defective Nrg1-ErbB4 signaling (Figure 5G). These results suggest that function of GluN2D in PVIs is a point of convergence of proteins and pathways critical for GABAergic signaling and those associated with SZ.

Hyperlocomotion and anxiety behaviors in mice with ablation of GluN2D from PV interneurons.

We next tested whether ablation of GluN2D from PVIs results in behavioral changes which may be relevant to SZ. In open field test to measure novelty-induced locomotor activity, PV-GluN2D KO mice showed significantly higher distance traveled (Figure 6A and A') as compared to the PV-cre WT. The time in center was significantly less in PV-GluN2D KO (PV-Cre = 158.7 ± 10.9 s vs PV-GluN2D KO = 118.3 ± 12.3 s). Moreover, in zero maze test, PV-GluN2D KO mice spent significantly less time in open zone (Figure 6B) with a trend for lower number of entries in open zone suggesting higher anxiety-like behavior. In forced swim test PV-GluN2D KO mice were found to have higher mobility time and lower immobility time suggesting lower depression-like behavior (Figure 6C and C'). In social interaction test a significantly higher time spent with animate side was observed in PV-GluN2D KO (Figure 6D). Further, PV-GluN2D KO showed shorter latency to fall in rotarod test suggesting motor incoordination (Figure S10A). Furthermore, PV-GluN2D KO appeared to be less responsive to MK-801 since the pre-MK-801 hyperlocomotion was absent after MK-801 injection suggesting that GluN2D in PVIs may partly underlie NMDA channel blocker-induced psychotic effects. No significant difference was observed in prepulse inhibition or startle response (Figure S10B–C). Together, these results demonstrate that deletion of GluN2D subunit from PVIs produces hyperactivity and anxiety-like behaviors relevant to SZ. In contrast, PV-GluN2D KO mice demonstrated lower depression-like behavior and an increase in social interaction suggesting lack of anhedonia or social deficits.

Deficit in short-term memory and cognitive flexibility in PV-GluN2D KO mice

We next examined the role of GluN2D in PVIs in cognitive function. We first examined short-term and long-term memory using the novel object recognition test. We found a significant reduction in the discrimination index in PV-GluN2D KO in the short-term but no change in long-term memory (Figure 6E). No change was found in percent alternations in Y-maze test (Figure S10D–D'). Spatial learning and behavioral flexibility were tested in the water T-Maze test. No significant difference was observed in PV-GluN2D KO mice in habit acquisition learning, however there was a trend for lower time to find the platform in PV-GluN2D KO mice suggesting intact cognition (Figure 6F1–F3). In contrast, during reversal learning PV-GluN2D KO mice more often entered the non-platform arm. The percent of error-free trials in reversal learning were significantly lower (Figure 6F4) and number of perseverative as well as total errors were significantly higher (Figure 6F5–6F6). Together, these results demonstrate significant cognitive dysfunction in PV-GluN2D KO mice especially in short-term memory and reversal learning.

Discussion

Over the years the NMDA receptor hypofunction hypothesis, based on the SZ symptomology produced by administration of NMDA channel blockers in humans, has been refined to suggest that NMDA receptors in interneurons may be a major contributor to SZ phenotypes. Specifically, these studies used model with conditional ablation of obligatory GluN1 subunit in PVIs using PV-Cre mouse line [15, 16, 18, 55, 56]. Using this strategy these studies found an important role of NMDA receptors in PVIs in cortical function and SZ-related behaviors. Here we found a critical role of GluN2D subunit in the PVIs in regulating neural circuitry, signaling and behaviors relevant to SZ. Recent neuroanatomical and electrophysiological studies have demonstrated expression of GluN2D subunits in cortico-limbic interneurons, including PVIs [25–27]. GluN2D-containing NMDA receptor have also been identified at both synaptic and extrasynaptic location in interneurons and PVIs which are tonically active and regulate cellular excitability [38, 57, 58]. Nonetheless, the precise subunit composition of NMDA receptors in PVIs in mPFC has not been systematically analyzed. We found that selective antagonists for GluN2C/2D and GluN2B produced more than 50% inhibition of currents whereas GluN2A selective inhibitor did not have a significant effect. In PV-GluN2D KO, GluN2C/2D antagonist produced no effect but GluN2A antagonist produced significant inhibition. Thus, PVIs primarily express GluN1/2B/2D receptors and loss of GluN2D does not eliminate NMDA receptor currents but changes the composition to GluN1/2A/2B.

Hyperexcitable state and inhibitory dysfunction in the mPFC upon GluN2D subunit ablation from PV interneurons

PVIs have been found to regulate excitability in the mPFC and changes in E-I balance has been noted in models of SZ [2, 11, 59, 60]. We found that in PV-GluN2D KO mice, pyramidal neurons were hyperexcitable whereas PVIs showed reduced excitability. Furthermore, we found that sEPSC frequency was higher in both PVIs and pyramidal neurons and vGluT1 level were upregulated supporting hyperexcitation in mPFC. In contrast to hyperexcitation, we found a specific alteration in the inhibitory system pointing to abnormalities in feed-forward inhibition. Specifically, we found that sIPSC frequency was significantly higher in pyramidal neurons but significantly lower in PVIs. Previous studies have found that the PVIs have a stronger input onto pyramidal neurons whereas SST neurons have major inputs to PVIs [41]. Our immunohistochemical analysis demonstrated higher PVI puncta and GAD67 colocalized puncta and a contrasting reduction in SST interneuron puncta and GAD67 colocalized puncta in PV-GluN2D KO. These findings support a model where PVI mediated inhibition on pyramidal neurons is increased and reduced SST inhibition of PVIs may further exaggerate feed-forward inhibition onto pyramidal neurons. Together these findings demonstrate that loss of GluN2D from PVIs initiates maladaptive changes in other cell types in the mPFC resulting in circuit dysfunction. It should be noted that the use of PV-Cre line in previous and our study leads to ablation of NMDA receptor subunit in PVIs in multiple brain regions which can contribute partly to the observed phenotypes.

Converging molecular changes relevant to SZ in PV-GluN2D KO mice

To delineate the molecular network of GluN2D-dependent circuit dysfunction relevant to SZ we performed transcriptomic analysis. Although the DEGs that we observed in the PV-GluN2D KO were limited, these pointed to key changes in inhibitory neurotransmission. For instance, we found a convergence of DEGs critical for GABAergic synapses, involving both presynaptic and postsynaptic molecules including Gad67, GABA transporter (Slc32a1 or vGAT), and GABA receptor (Gabra2). While the Gad67 and Slc32a1 were downregulated, which were consistent with the colocalization studies (Figure 3), surprisingly, Gabra2 was upregulated in the PV-GluN2D KO mice. Interestingly, Gabra2 is preferentially expressed at PVI-mediated axon-initial-segment inhibitory synapses onto pyramidal cells [61]. Thus, Gabra2 upregulation is consistent with our observation of an increase in PVI mediated inhibition of pyramidal neurons in PV-GluN2D KO mice (Figure 3). With regard to SZ, while reduced GAD67 in dorsolateral PFC is consistently observed in postmortem tissue from SZ patients [62, 63], reports also indicate an increase in Gabra2 in SZ [64, 65] which may be a compensatory mechanism to overcome reduced inhibition. Perturbations in GABAergic synapses were observed not only at functional level but also at the level of synaptogenesis. A significant reduction of inhibitory adhesion molecule Nlgn2 [66, 67] and synaptogenic molecules Cbln1, Cbln4 and GluD1 were found. Interestingly, Cbln4, together with its postsynaptic interacting partner GluD1, has been found to establish inhibitory synapses mediated by SST interneurons onto pyramidal neurons [68]. Consistent with this function, downregulation of Cbln4 and GluD1 was accompanied by a reduction in SST mediated GAD67+ve elements in PV-GluN2D KO (Figure 3). In addition to the inhibitory neurotransmission, GluN2D in PVIs may also be contributing to dopaminergic neurotransmission in the mPFC and thereby to the cognitive deficits (impaired short-term memory and behavioral flexibility) and positive symptoms (hyperlocomotion) relevant to SZ [69]. Specifically, we observed a reduction in dopamine synapse associated tyrosine hydroxylase (Th), dopamine transporter (Slc6a3), Dlx2 and Pax6. Finally, an increase in excitatory neurotransmission and vGluT1 expression demonstrate impairment in glutamatergic system in PV-GluN2D KO mice (Figure 1, 2). Thus, disruption in PV-GluN2D KO mice encompasses GABAergic, dopaminergic, and glutamatergic systems, all relevant to SZ pathophysiology. Another remarkable relationship of GluN2D in PVIs to SZ was observed in the downregulation of SZ-associated Nrg1, ErbB4 and Disc1 in PV-GluN2D KO mice. We strengthened the finding of downregulation of Nrg1-ErbB4 by studying downstream effectors Akt and mTOR, which were less active in PV-GluN2D KO mice. ErbB4 is enriched in PVIs and together with Nrg1 enhances excitatory synapse formation onto interneurons and inhibitory synapse formation onto pyramidal neurons [70, 71].

Refined NMDA receptor hypofunction hypothesis specific to GluN2D subunit

In conclusion, our electrophysiology results demonstrate that ablation of GluN2D subunit from PVIs primarily leads to a shift in the composition of NMDA receptor from GluN1/2B/2D to GluN1/2A/2B and not a significant change in current amplitude. Despite this, strong changes in circuit function, molecular networks and behaviors involving multiple neurotransmitter systems associated with SZ were observed in PV-GluN2D KO mice. Short-term memory and reversal learning deficits were observed in PV-GluN2D KO mice demonstrating cognitive impairment in a specific domain. It should however be noted that

we found no deficit in prepulse inhibition, reduced depression-like behavior and greater social interaction in PV-GluN2D KO mice (Table 1). In addition, we did not test whether gamma oscillations were affected in PV-GluN2D KO model, a phenomenon observed in SZ [12–14] and PVIs in the mPFC have been found to regulate gamma rhythms which regulate cognitive function and social behaviors [72]. We found that PVIs have stronger inhibitory control on pyramidal neurons which may account for the observed cognitive deficits and improved social behavior. In addition, GluN2B and GluN2A function in PVIs has been found to underlie antidepressant action of ketamine [73, 74]. The increase in GluN2A/2B contribution in PVI upon GluN2D deletion may produce antidepressant effect with higher mobile time in the forced swim test. Despite these limitations, our results demonstrate that not a simple NMDA receptor hypofunction, but a change in subunit composition can precipitate robust maladaptive changes in the mPFC function leading to behavioral consequences. Greater attention towards subunit specific roles of NMDA receptors is therefore needed to better understand the pathophysiology of SZ and other neurodevelopmental disorders.

Supplementary Material

Refer to Web version on PubMed Central for supplementary material.

Acknowledgement:

The authors are thankful to Bishal Misra and Patrick Andrews for excellent technical help.

Funding/Disclosures:

This work was supported by grants from the NSF1456818 (SMD), NIH NS104705 (SMD), NIH NS118731 (SMD) and NIH MH116003 (SMD).

References

1. Lisman JE, Coyle JT, Green RW, Javitt DC, Benes FM, Heckers S, et al. Circuit-based framework for understanding neurotransmitter and risk gene interactions in schizophrenia. Trends Neurosci 2008; 31: 234–42. [PubMed: 18395805]
2. Lisman J. Excitation, inhibition, local oscillations, or large-scale loops: What causes the symptoms of schizophrenia? Curr Opin Neurobiol 2012; 22: 537–44. [PubMed: 22079494]
3. Arnsten AF. Prefrontal cortical network connections: Key site of vulnerability in stress and schizophrenia. Int J Dev Neurosci 2011; 29: 215–23. [PubMed: 21345366]
4. Beasley CL, Reynolds GP. Parvalbumin-immunoreactive neurons are reduced in the prefrontal cortex of schizophrenics. Schizophr Res 1997; 24: 349–55. [PubMed: 9134596]
5. Woo TU, Miller JL, Lewis DA. Schizophrenia and the parvalbumin-containing class of cortical local circuit neurons. Am J Psychiatry 1997; 154: 1013–5. [PubMed: 9210755]
6. Reynolds GP, Beasley CL. GABAergic neuronal subtypes in the human frontal cortex--development and deficits in schizophrenia. J Chem Neuroanat 2001; 22: 95–100. [PubMed: 11470557]
7. Lewis DA, Cruz DA, Melchitzky DS, Pierri JN Lamina-specific deficits in parvalbumin-immunoreactive varicosities in the prefrontal cortex of subjects with schizophrenia: Evidence for fewer projections from the thalamus. Am J Psychiatry 2001; 158: 1411–22. [PubMed: 11532725]
8. Nakazawa K, Zsiros V, Jiang Z, Nakao K, Kolata S, Zhang S, et al. GABAergic interneuron origin of schizophrenia pathophysiology. Neuropharmacology 2012; 62: 1574–83. [PubMed: 21277876]
9. Akbarian S, Huang HS. Molecular and cellular mechanisms of altered GAD1/GAD67 expression in schizophrenia and related disorders. Brain Res Rev 2006; 52: 293–304. [PubMed: 16759710]

10. Gonzalez-Burgos G, Fish KN, Lewis DA. GABA neuron alterations, cortical circuit dysfunction and cognitive deficits in schizophrenia. Neural Plast 2011; 2011: 723184.
11. Gonzalez-Burgos G, Hashimoto T, Lewis DA. Alterations of cortical GABA neurons and network oscillations in schizophrenia. Curr Psychiatry Rep 2010; 12: 335–44. [PubMed: 20556669]
12. Lewis DA, Curley AA, Glausier JR, Volk DW. Cortical parvalbumin interneurons and cognitive dysfunction in schizophrenia. Trends Neurosci 2012; 35: 57–67. [PubMed: 22154068]
13. Marin O. Interneuron dysfunction in psychiatric disorders. Nat Rev Neurosci 2012; 13: 107–20. [PubMed: 22251963]
14. Uhlhaas PJ, Singer W. Neuronal dynamics and neuropsychiatric disorders: Toward a translational paradigm for dysfunctional large-scale networks. Neuron 2012; 75: 963–80. [PubMed: 22998866]
15. Carlen M, Meletis K, Siegle JH, Cardin JA, Futai K, Vierling-Claassen D, et al. A critical role for NMDA receptors in parvalbumin interneurons for gamma rhythm induction and behavior. Mol Psychiatry 2012; 17: 537–48. [PubMed: 21468034]
16. Korotkova T, Fuchs EC, Ponomarenko A, von Engelhardt J, Monyer H. NMDA receptor ablation on parvalbumin-positive interneurons impairs hippocampal synchrony, spatial representations, and working memory. Neuron 2010; 68: 557–69. [PubMed: 21040854]
17. Belforte JE, Zsiros V, Sklar ER, Jiang Z, Yu G, Li Y, et al. Postnatal NMDA receptor ablation in corticolimbic interneurons confers schizophrenia-like phenotypes. Nat Neurosci 2010; 13: 76–83. [PubMed: 19915563]
18. Billingslea EN, Tatard-Leitman VM, Anguiano J, Jutzeler CR, Suh J, Saunders JA, et al. Parvalbumin cell ablation of NMDA-R1 causes increased resting network excitability with associated social and selfcare deficits. Neuropsychopharmacology 2014; .
19. Kantrowitz JT, Javitt DC. N-methyl-d-aspartate (NMDA) receptor dysfunction or dysregulation: The final common pathway on the road to schizophrenia? Brain Res Bull 2010; 83: 108–21. [PubMed: 20417696]
20. Ross CA, Margolis RL, Reading SA, Pletnikov M, Coyle JT. Neurobiology of schizophrenia. Neuron 2006; 52: 139–53. [PubMed: 17015232]
21. Gilmour G, Dix S, Fellini L, Gastambide F, Plath N, Steckler T, et al. NMDA receptors, cognition and schizophrenia--testing the validity of the NMDA receptor hypofunction hypothesis. Neuropharmacology 2012; 62: 1401–12. [PubMed: 21420987]
22. Marek GJ, Behl B, Bespalov AY, Gross G, Lee Y, Schoemaker H. Glutamatergic (N-methyl-D-aspartate receptor) hypofrontality in schizophrenia: Too little juice or a miswired brain? Mol Pharmacol 2010; 77: 317–26. [PubMed: 19933774]
23. Alsaad HA, DeKorver NW, Mao Z, Dravid SM, Arikkath J, Monaghan DT. In the telencephalon, GluN2C NMDA receptor subunit mRNA is predominately expressed in glial cells and GluN2D mRNA in interneurons. Neurochem Res 2019; 44: 61–77. [PubMed: 29651654]
24. Ravikrishnan A, Gandhi PJ, Shelkar GP, Liu J, Pavuluri R, Dravid SM. Region-specific expression of NMDA receptor GluN2C subunit in parvalbumin-positive neurons and astrocytes: Analysis of GluN2C expression using a novel reporter model. Neuroscience 2018; 380: 49–62. [PubMed: 29559384]
25. Perszyk RE, DiRaddo JO, Strong KL, Low CM, Ogden KK, Khatri A, et al. GluN2D-containing N-methyl-d-aspartate receptors mediate synaptic transmission in hippocampal interneurons and regulate interneuron activity. Mol Pharmacol 2016; 90: 689–702. [PubMed: 27625038]
26. von Engelhardt J, Bocklisch C, Tonges L, Herb A, Mishina M, Monyer H. GluN2D-containing NMDA receptors-mediate synaptic currents in hippocampal interneurons and pyramidal cells in juvenile mice. Front Cell Neurosci 2015; 9: 95. [PubMed: 25859181]
27. Yamasaki M, Okada R, Takasaki C, Toki S, Fukaya M, Natsume R, et al. Opposing role of NMDA receptor GluN2B and GluN2D in somatosensory development and maturation. J Neurosci 2014; 34: 11534–48.
28. Monyer H, Burnashev N, Laurie DJ, Sakmann B, Seeburg PH. Developmental and regional expression in the rat brain and functional properties of four NMDA receptors. Neuron 1994; 12: 529–40. [PubMed: 7512349]

29. Traynelis SF, Wollmuth LP, McBain CJ, Menniti FS, Vance KM, Ogden KK, et al. Glutamate receptor ion channels: Structure, regulation, and function. Pharmacol Rev 2010; 62: 405–96. [PubMed: 20716669]
30. Sapkota K, Mao Z, Synowicki P, Lieber D, Liu M, Ikezu T, et al. GluN2D N-methyl-d-aspartate receptor subunit contribution to the stimulation of brain activity and gamma oscillations by ketamine: Implications for schizophrenia. J Pharmacol Exp Ther 2016; 356: 702–11. [PubMed: 26675679]
31. Mao Z, He S, Mesnard C, Synowicki P, Zhang Y, Chung L, et al. NMDA receptors containing GluN2C and GluN2D subunits have opposing roles in modulating neuronal oscillations; potential mechanism for bidirectional feedback. Brain Res 2020; 1727: 146571.
32. Yuan H, Low CM, Moody OA, Jenkins A, Traynelis SF. Ionotropic GABA and glutamate receptor mutations and human neurologic diseases. Mol Pharmacol 2015; 88: 203–17. [PubMed: 25904555]
33. Makino C, Shibata H, Ninomiya H, Tashiro N, Fukumaki Y. Identification of single-nucleotide polymorphisms in the human N-methyl-D-aspartate receptor subunit NR2D gene, GRIN2D, and association study with schizophrenia. Psychiatr Genet 2005; 15: 215–21. [PubMed: 16094258]
34. Liu J, Shelkar GP, Sarode LP, Gawande DY, Zhao F, Clausen RP, et al. Facilitation of GluN2C-containing NMDA receptors in the external globus pallidus increases firing of fast spiking neurons and improves motor function in a hemiparkinsonian mouse model. Neurobiol Dis 2021; 150: 105254.
35. Gawande DY, Shelkar GP, Liu J, Ayala AD, Pavuluri R, Choi D, et al. Glutamate delta-1 receptor regulates inhibitory neurotransmission in the nucleus accumbens core and anxiety-like behaviors. Mol Neurobiol 2021; 58: 4787–801. [PubMed: 34173171]
36. Liu J, Shelkar GP, Gandhi PJ, Gawande DY, Hoover A, Villalba RM, et al. Striatal glutamate delta-1 receptor regulates behavioral flexibility and thalamostriatal connectivity. Neurobiol Dis 2020; 137: 104746.
37. Shelkar GP, Liu J, Dravid SM. Astrocytic NMDA receptors in the basolateral amygdala contribute to facilitation of fear extinction. Int J Neuropsychopharmacol 2021; .
38. Garst-Orozco J, Malik R, Lanz TA, Weber ML, Xi H, Arion D, et al. GluN2D-mediated excitatory drive onto medial prefrontal cortical PV+ fast-spiking inhibitory interneurons. PLoS One 2020; 15: e0233895.
39. Salimando GJ, Hyun M, Boyt KM, Winder DG. BNST GluN2D-containing NMDA receptors influence anxiety- and depressive-like behaviors and ModulateCell-specific excitatory/inhibitory synaptic balance. J Neurosci 2020; 40: 3949–68. [PubMed: 32277042]
40. Kaneko T, Fujiyama F. Complementary distribution of vesicular glutamate transporters in the central nervous system. Neurosci Res 2002; 42: 243–50. [PubMed: 11985876]
41. Cummings KA, Clem RL. Prefrontal somatostatin interneurons encode fear memory. Nat Neurosci 2020; 23: 61–74. [PubMed: 31844314]
42. Zhou Y, Zhou B, Pache L, Chang M, Khodabakhshi AH, Tanaseichuk O, et al. Metascape provides a biologist-oriented resource for the analysis of systems-level datasets. Nat Commun 2019; 10: 1523–6. [PubMed: 30944313]
43. Koopmans F, van Nierop P, Andres-Alonso M, Byrnes A, Cijsouw T, Coba MP, et al. SynGO: An evidence-based, expert-curated knowledge base for the synapse. Neuron 2019; 103: 217,234.e4.
44. Chen J, Bardes EE, Aronow BJ, Jegga AG. ToppGene suite for gene list enrichment analysis and candidate gene prioritization. Nucleic Acids Res 2009; 37: 305.
45. Volk DW, Austin MC, Pierri JN, Sampson AR, Lewis DA. Decreased glutamic acid decarboxylase67 messenger RNA expression in a subset of prefrontal cortical gamma-aminobutyric acid neurons in subjects with schizophrenia. Arch Gen Psychiatry 2000; 57: 237–45. [PubMed: 10711910]
46. Impagnatiello F, Guidotti AR, Pesold C, Dwivedi Y, Caruncho H, Pisu MG, et al. A decrease of reelin expression as a putative vulnerability factor in schizophrenia. Proc Natl Acad Sci U S A 1998; 95: 15718–23.

47. Guidotti A, Auta J, Davis JM, Di-Giorgi-Gerevini V, Dwivedi Y, Grayson DR, et al. . Decrease in reelin and glutamic acid decarboxylase67 (GAD67) expression in schizophrenia and bipolar disorder: A postmortem brain study. Arch Gen Psychiatry 2000; 57: 1061–9. [PubMed: 11074872]
48. Norton N, Moskvina V, Morris DW, Bray NJ, Zammit S, Williams NM, et al. Evidence that interaction between neuregulin 1 and its receptor erbB4 increases susceptibility to schizophrenia. Am J Med Genet B Neuropsychiatr Genet 2006; 141B: 96–101. [PubMed: 16249994]
49. Kamiya A, Kubo K, Tomoda T, Takaki M, Youn R, Ozeki Y, et al. A schizophrenia-associated mutation of DISC1 perturbs cerebral cortex development. Nat Cell Biol 2005; 7: 1167–78. [PubMed: 16299498]
50. Millar JK, Christie S, Semple CA, Porteous DJ. Chromosomal location and genomic structure of the human translin-associated factor X gene (TRAX; TSNAX) revealed by intergenic splicing to DISC1, a gene disrupted by a translocation segregating with schizophrenia. Genomics 2000; 67: 69–77. [PubMed: 10945471]
51. Sun C, Cheng M, Qin R, Liao D, Chen T, Koong F, et al. Identification and functional characterization of rare mutations of the neuroligin-2 gene (NLGN2) associated with schizophrenia. Hum Mol Genet 2011; 20: 3042–51. [PubMed: 21551456]
52. Stefansson H, Sigurdsson E, Steinthorsdottir V, Bjornsdottir S, Sigmundsson T, Ghosh S, et al. Neuregulin 1 and susceptibility to schizophrenia. Am J Hum Genet 2002; 71: 877–92. [PubMed: 12145742]
53. Saunders A, Macosko EZ, Wysoker A, Goldman M, Krienen FM, de Rivera H, et al. Molecular diversity and specializations among the cells of the adult mouse brain. Cell 2018; 174: 1015,1030.e16. [PubMed: 30096299]
54. Seshadri S, Faust T, Ishizuka K, Delevich K, Chung Y, Kim S, et al. Interneuronal DISC1 regulates NRG1-ErbB4 signalling and excitatory-inhibitory synapse formation in the mature cortex. Nat Commun 2015; 6: 10118.
55. Bygrave AM, Masiulis S, Nicholson E, Berkemann M, Barkus C, Sprengel R, et al. Knockout of NMDA-receptors from parvalbumin interneurons sensitizes to schizophrenia-related deficits induced by MK-801. Transl Psychiatry 2016; 6: e778. [PubMed: 27070406]
56. Saunders JA, Tatard-Leitman VM, Suh J, Billingslea EN, Roberts TP, Siegel SJ. Knockout of NMDA receptors in parvalbumin interneurons recreates autism-like phenotypes. Autism Res 2013; 6: 69–77. [PubMed: 23441094]
57. Yao L, Rong Y, Ma X, Li H, Deng D, Chen Y, et al. Extrasynaptic NMDA receptors bidirectionally modulate intrinsic excitability of inhibitory neurons. J Neurosci 2022; 42: 3066–79. [PubMed: 35197319]
58. Hanson E, Armbruster M, Lau LA, Sommer ME, Klaft ZJ, Swanger SA, et al. Tonic activation of GluN2C/GluN2D-containing NMDA receptors by ambient glutamate facilitates cortical interneuron maturation. J Neurosci 2019; 39: 3611–26. [PubMed: 30846615]
59. Homayoun H, Moghaddam B. NMDA receptor hypofunction produces opposite effects on prefrontal cortex interneurons and pyramidal neurons. J Neurosci 2007; 27: 11496–500.
60. Lewis DA, Curley AA, Glausier JR, Volk DW. Cortical parvalbumin interneurons and cognitive dysfunction in schizophrenia. Trends Neurosci 2012; 35: 57–67. [PubMed: 22154068]
61. Nusser Z, Sieghart W, Benke D, Fritschy JM, Somogyi P. Differential synaptic localization of two major gamma-aminobutyric acid type A receptor alpha subunits on hippocampal pyramidal cells. Proc Natl Acad Sci U S A 1996; 93: 11939–44.
62. Thompson M, Weickert CS, Wyatt E, Webster MJ. Decreased glutamic acid decarboxylase(67) mRNA expression in multiple brain areas of patients with schizophrenia and mood disorders. J Psychiatr Res 2009; 43: 970–7. [PubMed: 19321177]
63. Curley AA, Arion D, Volk DW, Asafu-Adjei JK, Sampson AR, Fish KN, et al. Cortical deficits of glutamic acid decarboxylase 67 expression in schizophrenia: Clinical, protein, and cell type-specific features. Am J Psychiatry 2011; 168: 921–9. [PubMed: 21632647]
64. Benes FM, Vincent SL, Marie A, Khan Y. Up-regulation of GABAA receptor binding on neurons of the prefrontal cortex in schizophrenic subjects. Neuroscience 1996; 75: 1021–31. [PubMed: 8938738]

65. Volk DW, Pierri JN, Fritschy J, Auh S, Sampson AR, Lewis DA. Reciprocal alterations in pre- and postsynaptic inhibitory markers at chandelier cell inputs to pyramidal neurons in schizophrenia. Cereb Cortex 2002; 12: 1063–70. [PubMed: 12217970]

66. Chubykin AA, Atasoy D, Etherton MR, Brose N, Kavalali ET, Gibson JR, et al. Activity-dependent validation of excitatory versus inhibitory synapses by neuroligin-1 versus neuroligin-2. Neuron 2007; 54: 919–31. [PubMed: 17582332]

67. Liang J, Xu W, Hsu Y, Yee AX, Chen L, Sudhof TC. Conditional knockout of Nlgn2 in the adult medial prefrontal cortex (mPFC) induces delayed loss of inhibitory synapses. Mol Psychiatry 2015; 20: 793. [PubMed: 26098222]

68. Fossati M, Assendorp N, Gemin O, Colasse S, Dingli F, Arras G, et al. Trans-synaptic signaling through the glutamate receptor delta-1 mediates inhibitory synapse formation in cortical pyramidal neurons. Neuron 2019; 104: 1081,1094.e7.

69. Jentsch JD, Roth RH. The neuropsychopharmacology of phencyclidine: From NMDA receptor hypofunction to the dopamine hypothesis of schizophrenia. Neuropsychopharmacology 1999; 20: 201–25. [PubMed: 10063482]

70. Fazzari P, Paternain AV, Valiente M, Pla R, Lujan R, Lloyd K, et al. Control of cortical GABA circuitry development by Nrg1 and ErbB4 signalling. Nature 2010; 464: 1376–80. [PubMed: 20393464]

71. Del Pino I, Garcia-Frigola C, Dehorter N, Brotons-Mas JR, Alvarez-Salvado E, Martinez de Lagran M, et al. Erbb4 deletion from fast-spiking interneurons causes schizophrenia-like phenotypes. Neuron 2013; 79: 1152–68. [PubMed: 24050403]

72. Sohal VS, Zhang F, Yizhar O, Deisseroth K. Parvalbumin neurons and gamma rhythms enhance cortical circuit performance. Nature 2009; 459: 698–702. [PubMed: 19396159]

73. Gerhard DM, Pothula S, Liu R, Wu M, Li X, Girgenti MJ, et al. GABA interneurons are the cellular trigger for ketamine's rapid antidepressant actions. J Clin Invest 2020; 130: 1336–49. [PubMed: 31743111]

74. Picard N, Takesian AE, Fagiolini M, Hensch TK. NMDA 2A receptors in parvalbumin cells mediate sex-specific rapid ketamine response on cortical activity. Mol Psychiatry 2019; 24: 828–38. [PubMed: 30696941]

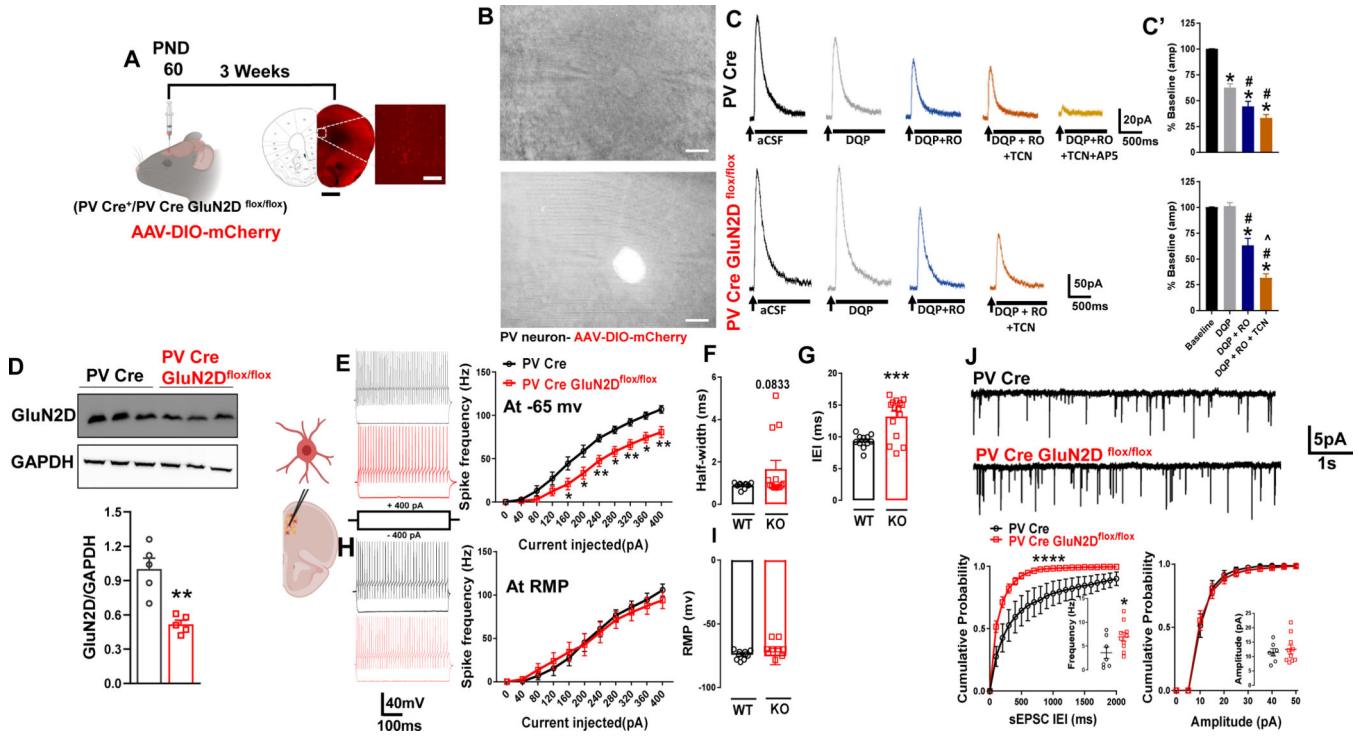

Figure 1. PVIs express GluN1/2B/2D receptors which regulate PVI excitability and excitatory neurotransmission.

(A) Labeling of PVIs was performed by infusion of Cre-dependent AAV-DIO-mCherry on postnatal day (PND) 60 (left). Injection site and mCherry expression in PVIs was observed in the mPFC. **(B)** Contrast images showing mCherry expressing PVIs and the position of recording and puff pipette (top). **(C)** Brief pulses (10–15 ms) of glutamate (1 mM) and glycine (100 μM) were applied using Picospritzer onto PVIs in acute brain slices and current responses were recorded by whole-cell voltage-clamp (V_{HOLD} +40 mV). Representative traces show puff-induced current responses which are blocked by subunit selective NMDA receptor inhibitors in PV Cre and PV Cre GluN2D$^{flox/flox}$ mice (right). **(C')** Effects of bath application of DQP 1105 (20 μM) (GluN2C/2D subunit antagonist), RO 25–6981 (10 μM) (GluN2B subunit antagonist), and TCN 201 (10 μM) (GluN2A subunit antagonist) on the peak amplitudes of current responses were plotted as the percentage of baseline aCSF responses. In PV Cre mice bath application of DQP 1105 significantly reduces the amplitude (% baseline) compared to the aCSF (*: as compared with aCSF; $p<0.0001$), further combination of DQP 1105 + RO 25–6981 significantly reduced the amplitude compared to the aCSF and DQP 1105 alone group (*: as compared with aCSF; $p<0.0001$, #: as compared with DQP 1105; $p<0.01$), one-way ANOVA, n = 6–13 PV neurons per group). In PV Cre GluN2D$^{flox/flox}$ mice bath application of DQP 1105 did not affect the amplitude compared to the aCSF (*: as compared with aCSF; $p>0.9999$), further combination of DQP 1105 + RO 25–6981 significantly reduced the amplitude compared to the aCSF and DQP 1105 (*: as compared with aCSF; $p<0.0001$, #: as compared with DQP 1105; $p<0.0001$)). The combination of DQP 1105 + RO 25–6981 + TCN 201 significantly reduced the amplitude compared to aCSF, DQP 1105, and DQP 1105 + RO 25–6981 combination (*: as compared with aCSF; $p<0.0001$, #: as compared with DQP 1105; $p<0.0001$), ^: as compared with DQP

1105 + RO 25–6981; p<0.0001), one-way ANOVA, n = 6–15 PVIs per group). **(D)** Western blotting analysis of synaptoneurosome protein from PV Cre and PV Cre GluN2D$^{flox/flox}$ mice mPFC. A significant reduction was observed in conditional deletion model (*p<0.01, unpaired t-test, n = 5 per group). **(E)** Schematic of whole-cell electrophysiology recordings of mCherry^{+} PVIs in mPFC (left). Representative current-clamp recording traces of fast spiking mCherry^{+} PVIs to current injections of −400 to +400 pA when the membrane potential was normalized to −65 mV. Average AP frequency in response to −400 to +400 pA depolarizing current steps illustrating a significant reduction in PVI excitability in PV Cre GluN2D$^{flox/flox}$ mice compared with PV-Cre mice (Two-way repeated measures ANOVA, genotype F (1, 273) = 63.92 p < 0.0001; Bonferroni's multiple comparisons test: PV Cre vs. PV Cre GluN2D$^{flox/flox}$, *p<0.05; **p<0.01, n = 11–17 cells from 5–6 mice). **(F)** No change in half width (n = 10–13 cells from 3 mice per group, p=0.8468, unpaired t-test). **(G)** A significantly higher inter event interval time was observed in PV Cre GluN2D $^{flox/flox}$ mice as compared to the PV Cre mice (n = 11–15 cells from 3 mice per group, ***p = 0.0003, unpaired t-test:). **(H)** No difference in the excitability of PVIs in the two genotypes when current-clamp recordings were obtained at resting membrane potential. **(I)** Resting membrane potential was unaltered between genotypes (n = 10–13 cells from 3 mice per group, p=0.0833, unpaired t-test). **(J)** Representative traces of spontaneous EPSCs recorded from PVIs (top), cumulative plots and scatter plots of frequency and amplitude (bottom) from PV Cre and PV Cre GluN2D $^{flox/flox}$ mice. A significantly higher sEPSC frequency was observed in PV Cre GluN2D $^{flox/flox}$ (*p = 0.0414, unpaired t-test). Inter-event interval (IEI) was also significantly lower (****p = 0.0001, K-S test). No change in amplitude was observed (p = 0.6269, n = 7–11 cells from 3 mice per group Unpaired t-test).

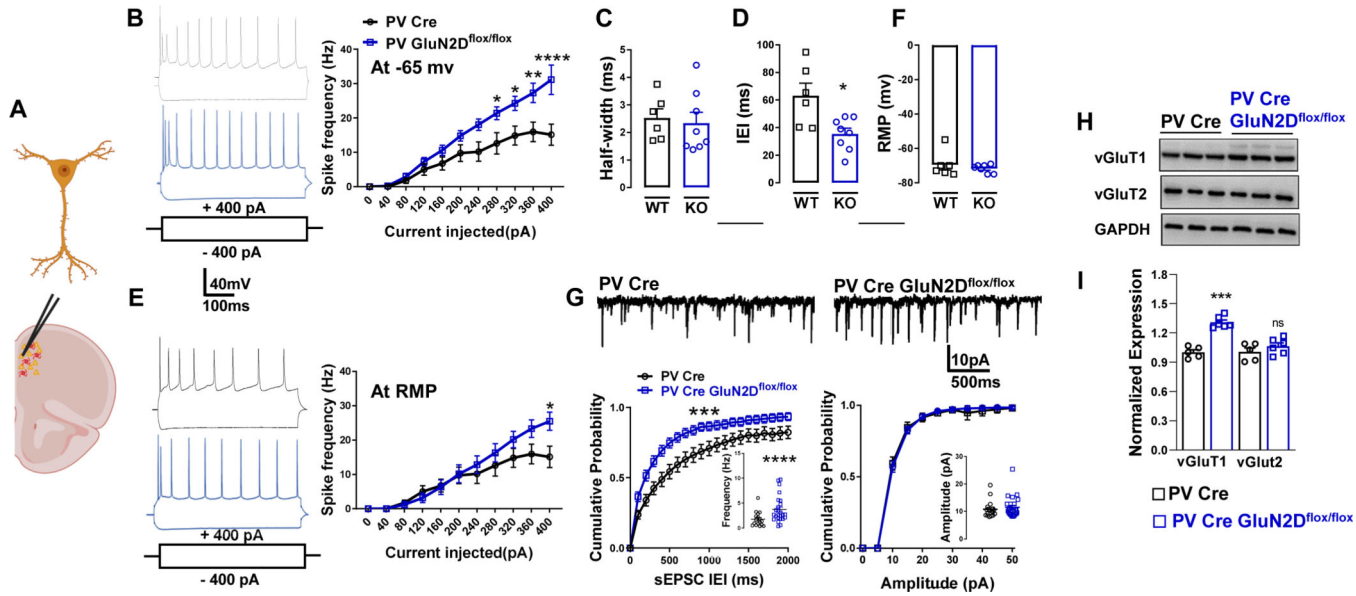

Figure 2. Pyramidal neurons in mPFC of PV-GluN2D KO are hyperexcitable and have higher excitatory neurotransmission.

(A) Schematic of whole-cell electrophysiology recordings from pyramidal neurons in mPFC (left). **(B)** Representative traces of PV Cre (top) and PV Cre GluN2D $^{flox/flox}$ (bottom) pyramidal neurons to current injections of −400 to +400 pA (right). At constant holding membrane potential (−65 mV) average AP frequency illustrating a significant increase in pyramidal neuron excitability in PV Cre GluN2D $^{flox/flox}$ mice compared with PV-Cre mice (Two-way repeated measures ANOVA, genotype F (1, 175) = 44.23 p < 0.0001; Bonferroni's multiple comparisons test: PV Cre vs. PV Cre GluN2D$^{flox/flox}$, *p<0.05; **p<0.01; ****p<0.0001, n = 8–10 cells from 4 mice per group). **(C)** Half width was unaltered in PV Cre GluN2D $^{flox/flox}$ (p = 0.7134). **(D)** A significantly lower inter event interval time was observed in PV Cre GluN2D $^{flox/flox}$ mice as compared to the PV Cre mice (*p = 0.026, unpaired t-test, n = 6–8 cells from 3 mice per group). **(E)** Representative traces of PV Cre (top) and PV Cre GluN2D $^{flox/flox}$ (bottom) pyramidal neurons to current injections of −400 to +400 pA (right). At resting membrane potential (−65 mV) average AP frequency in response to −400 to 400 pA depolarizing current steps illustrating a significant increase in pyramidal neuron excitability in PV Cre GluN2D $^{flox/flox}$ mice compared with PV-Cre mice (genotype F (1, 142) = 7.103 p<0.0086; Two-way repeated measures ANOVA, Bonferroni's multiple comparisons test: PV Cre vs. PV Cre GluN2D$^{flox/flox}$, *p<0.05, n = 7–8 cells from 4 mice per group). **(F)** Resting membrane potential was unaltered in PV Cre GluN2D $^{flox/flox}$ (p = 0.5095, unpaired t-test, n = 6–8 cells from 3 mice per group). **(G)** Representative traces of spontaneous EPSCs recorded in pyramidal neurons, cumulative plots and bar graphs of frequency and amplitude from PV Cre and PV Cre GluN2D $^{flox/flox}$ mice. A significantly higher sEPSC frequency was observed in PV Cre GluN2D $^{flox/flox}$ (**p = 0.0095, unpaired t-test). Inter-event interval (IEI) was also significantly lower (****p = 0.0006, K-S test). No change in amplitude was observed (p = 0.5148, unpaired t-test, n = 17–25 cells from 5–6 mice per group).

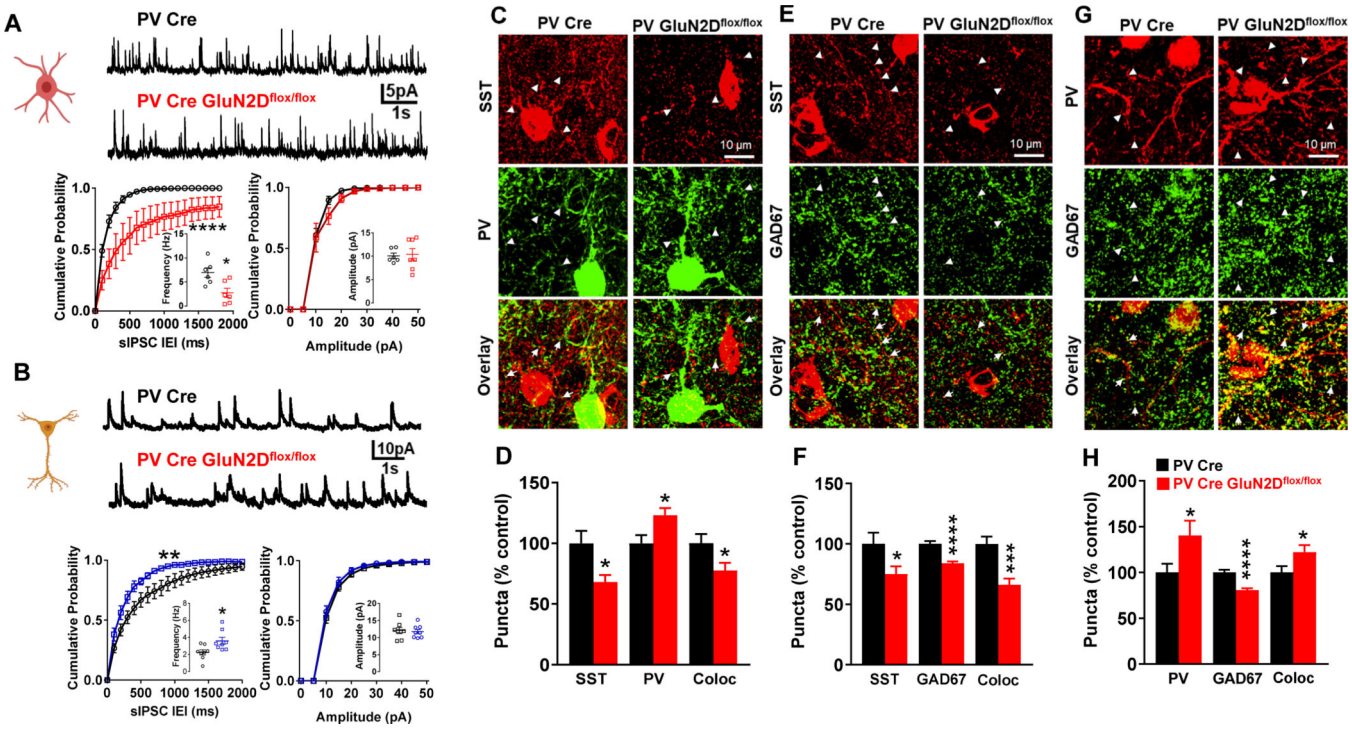

Figure 3. Ablation of GluN2D from PVIs reduces SST interneuron mediated inhibitory elements but increases PVI mediated inhibitory elements and inhibitory neurotransmission in pyramidal neurons.

(A) Schematic of whole-cell electrophysiology recordings of mCherry^{+} PVIs from L-2/3 in mPFC (left). Representative traces of sIPSCs recorded from PV Cre (top) and PV Cre GluN2D$^{flox/flox}$ (bottom) fast spiking mCherry^{+} PVIs, cumulative plots and bar graphs of frequency and amplitude from PV Cre and PV Cre GluN2D $^{flox/flox}$ mice. A significantly lower sIPSC frequency was observed in PV Cre GluN2D $^{flox/flox}$ (*p = 0.0125, unpaired t-test). Inter-event interval (IEI) was also significantly decreased (****p = 0.0001, K-S test). No change in amplitude was observed (p = 0.8304, n = 6 cells from 3 mice per genotype). **(B)** Cartoon depicting whole-cell recording from pyramidal neuron in L-2/3 in mPFC region. Representative traces of spontaneous sIPSCs recorded from pyramidal neurons, cumulative plots and bar graphs of frequency and amplitude from PV Cre and PV Cre GluN2D $^{flox/flox}$ mice A significantly higher sIPSC frequency was observed in PV Cre GluN2D $^{flox/flox}$ (*p = 0.0207, unpaired t-test). Inter-event interval (IEI) was also significantly decreased (**p = 0.0021, K-S test). No change in amplitude was observed (p = 0.7882, unpaired t-test, n = 8 cells from 3 mice per genotype). **(C)** Representative confocal images from mPFC of PV Cre and PV Cre GluN2D$^{flox/flox}$ mice immunostained for SST and PV. **(D)** Quantification of immunostaining; A significant reduction in the SST puncta (*p = 0.0106; unpaired t-test) and SST/PV colocalized puncta (*p = 0.0367; unpaired t-test), and increase in PV puncta (*p = 0.0156; unpaired t-test) following the ablation of GluN2D from PVIs. **C.** Confocal images from mPFC of PV Cre and PV CreGluN2D$^{flox/flox}$ mice immunostained for SST and GAD67. **(E)** Quantification of immunostaining; ablation of GluN2D from PVIs resulted in a significant reduction in SST puncta (*p = 0.0343; unpaired ttest), GAD 67 puncta (****p < 0.0001; unpaired t-test) and SST/GAD67 colocalized

puncta (***p = 0.0004; unpaired t-test). **(F)** Representative confocal images from mPFC of PV Cre and PV CreGluN2D$^{flox/flox}$ mice immunostained for PV and GAD67. **(G)** Quantification of immunostaining; A significant increase in the PV puncta, *p = 0.0383; unpaired t-test) and PV/GAD67 colocalized puncta (*p = 0.0453; unpaired t-test), and reduction in GAD67 puncta (****p < 0.0001; unpaired t-test) following ablation of GluN2D from PVIs. Arrowheads indicates individual puncta and arrows indicates colocalized puncta for the respective image panels. Data from n = 5 mice/group was collated and plotted as mean ± SEM.

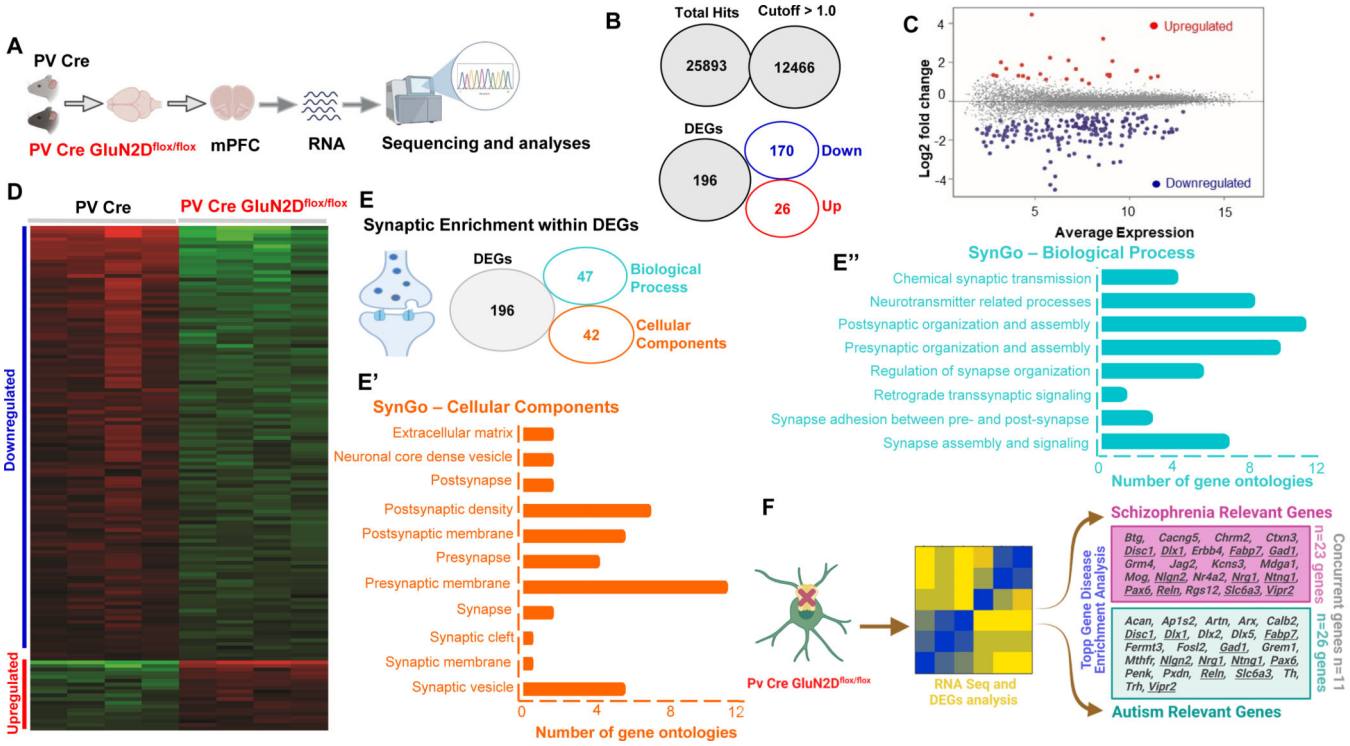

Figure 4. Transcriptomic and synaptic enrichment analysis of mPFC from Pv Cre and Pv Cre GluN2D$^{flox/flox}$ revealed genes relevant to inhibitory signaling, psychiatric and neurodevelopmental disorders.

(A) Bulk RNAseq workflow, briefly RNA was isolated from mPFC region dissected from the PV Cre control and PV Cre GluN2D$^{flox/flox}$ animals and subjected to sequencing in Novoseq6000 platform. **(B)** A total of 25893 genes were detected which were filtered based on the FPKM values (Cutoff ≥ 1) that led to 12466 genes from which 196 differentially expressed genes (DEGs) were identified. From this 196, 170 genes were downregulated and 26 were upregulated. **(C)** MA-plot of the entire sequencing results highlighting the differentially expressed genes (DEGs), upregulated (red) downregulated (blue) and nonsignificant (grey) genes. **(D)** Heatmap of DEGs between PV Cre and PV Cre GluN2D$^{flox/flox}$. **(E)** Venn diagram describing the synaptic enrichment of the identified 196 DEGs. The identified DEGs were subjected to SynGo analysis; 42-genes matches with SynGo cellular components and 47-genes that matches with SynGo biological process annotations. **(E', E")** Row-chart describing the genes associated with multiple cellular components and the biological processes within the synapse. **(E')** In the cellular components, the "Presynaptic cellular component" topped the list with 11 gene ontologies and 10 genes *Ntng1, Gabra2, Grm4, Nrg1, Chrm2, Vapa, Slc6a3, Vapa, Adcy8, Erbb4*. **(E")** In the biological process, the "Postsynaptic organization and assembly" topped the list with 12 gene ontologies and 8 genes *Nrg1, Syt6, Nlgn2, Gabra2, Tenm3, Disc1, Cbln1, Cacng5*. **(F)** Schematic representation of the genes relevant to schizophrenia and autism. The DEGs from RNA-seq were further subjected to Topp gene analysis for disease-specific enrichment. A total of 23-candidate genes for schizophrenia (SZ) and 26-candidate genes for autism spectrum disorder (ASD) were identified within the 196 DEGs. There were 11 genes (underlined in the box) which overlapped between SZ and ASD.

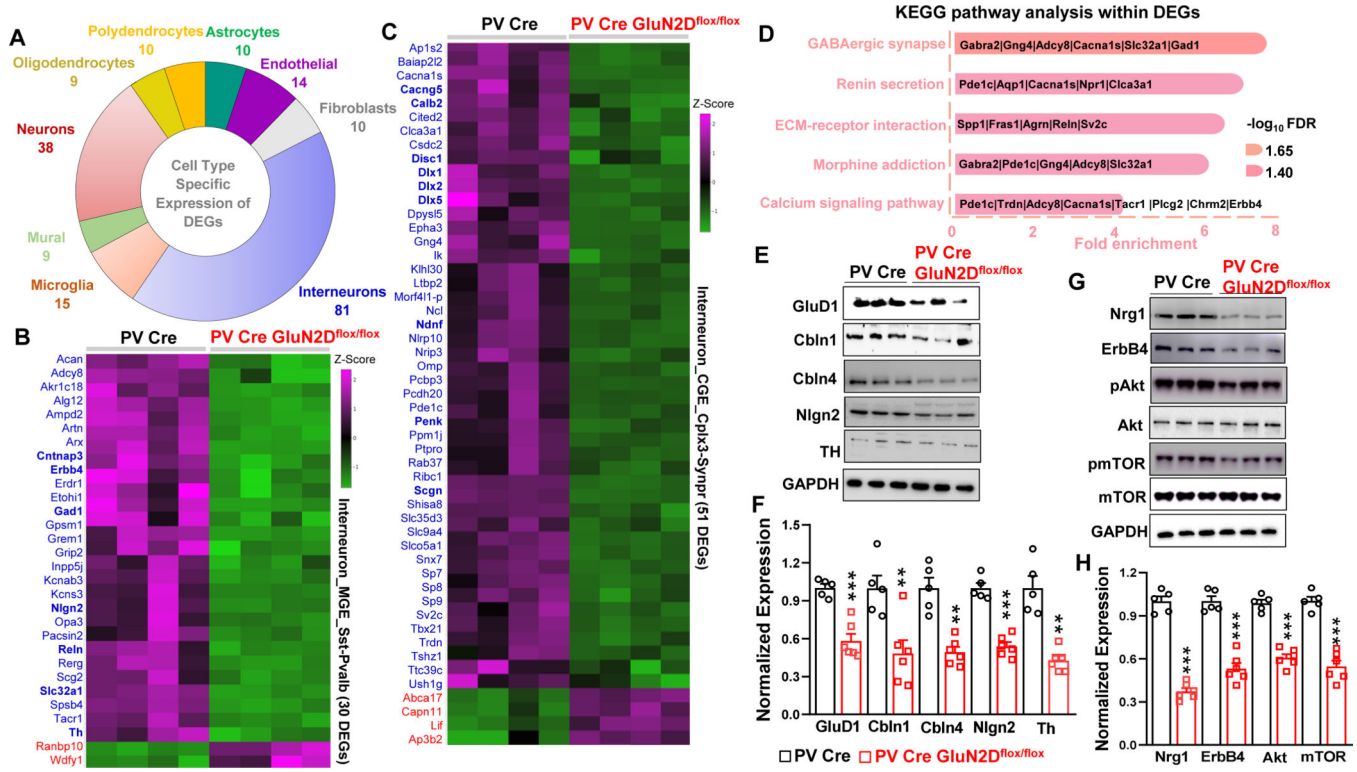

Figure 5. Cell-type specific enrichment and KEGG-pathway analysis of the DEGs outlined the impairment of the inhibitory signaling upon GluN2D deletion

(A) Donut chart visualization of the cell-type specific expression of the identified DEGs. Each color in the donut chart represents a specific cell type and among those interneuron specific genes topped the list with 81-genes followed by neurons with 38-genes within 196 DEGs. **(B, C)** Heatmaps showing interneuron specific DEGs. **(B)** Heatmaps of DEGs specific to MGE SST-Pvalb cluster of interneurons (N=30 genes). **(C)** Heatmaps of DEGs specific to CGE Cplx3-Synpr cluster of interneurons (N=51 genes). **(D)** KEGG pathway enrichment analysis within the DEGs identified top 5 pathways including GABAergic synapse, renin secretion, ECM-receptor interaction, morphine addiction and calcium signaling. Genes involved in each pathway are mentioned in the row-chart. **(E-H)** Validation of some of the identified DEGs through immunoblotting from the mPFC synaptoneurosomes of PV Cre and PV Cre GluN2D$^{flox/flox}$ (N = 5−6 mice). **(E)** Immunoblot analysis of transsynaptic molecules GluD1, Cbln1, Cbln4 and Nlgn2 and TH. Loss of GluN2D leads to downregulation of Cbln1, Cbln4, Nlgn2 and TH matching with the RNASeq data. In addition, GluD1, binding partner for Cbln1/Cbln4 is also downregulated in these animals. **(F)** Respective densitometries of GluD1 ($p = 0.0003$), Cbln1 ($p = 0.0063$), Cbln4 ($p = 0.0015$), Nlgn2 ($p = 0.0001$), and TH ($p = 0.0021$; unpaired t-test). **(G)** Immunoblot analysis of Nrg1, ErbB4, phospho and non-phospho forms of Akt and mTOR. Deletion of GluN2D in PVIs leads to downregulation of NRG1 and ErbB4 in the mPFC matching with the RNASeq data. Downregulation of NRG1-ErbB4 signaling was further confirmed by determining the activation of its downstream effectors Akt and mTOR. Both phosphor-Akt and phosphor-mTOR is significantly reduced in the PV Cre GluN2D$^{flox/flox}$ compared to PV Cre mice. **(F)** Respective densitometries of Nrg1 ($p < 0.0001$), ErbB4 ($p < 0.0001$), pAkt/Akt ($p < 0.0001$)

and pmTOR/mTOR ($p < 0.0001$; unpaired t-test). The densitometries for Akt and mTOR is represented as the ratio between the phospho form to the non-phospho form.

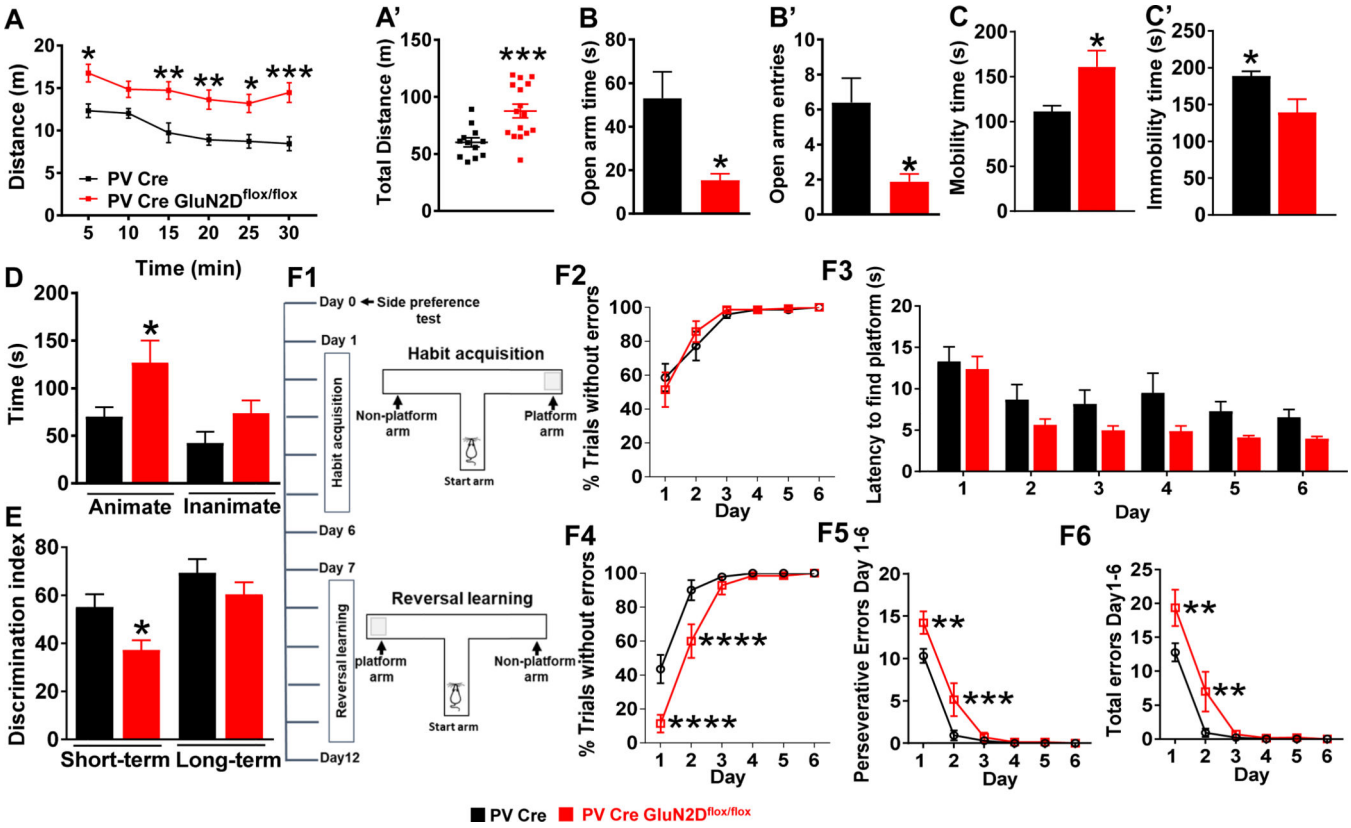

Figure 6. Hyperactivity, anxiety behavior and cognitive deficits in mice with GluN2D ablation from PVIs.

(A and A') Spontaneous locomotion evaluation in open filed test: **(A)** Average distance travelled over 30 min aggregated in 5-min bins. PV Cre GluN2D$^{flox/flox}$ mice travelled more distance during spontaneous locomotion evaluation than PV Cre (Two-way repeated measures ANOVA, genotype F (1, 26) = 12.98, p = 0.0013; Bonferroni's multiple comparisons test). Bonferroni's post-hoc test revealed a significant difference in distance travelled in PV Cre GluN2D$^{flox/flox}$ mice (5 min: *p = 0.0131; 15 min: **p = 0.0036; 20 min: p = **0.0067; 25 min: p = **0.0123; 30 min: ***p = 0.0002). **(A')** In total distance traveled PV Cre GluN2D$^{flox/flox}$ mice showed significantly more distance traveled compared to the PV Cre mice (**p = 0.0013, unpaired t-test, n = 12–16 mice per group). **(B and B')** In zero maze test, PV Cre GluN2D$^{flox/flox}$ mice showed significantly less time spent in open arm compared to the PV Cre mice and trend for lower entries (open arm time, *p = 0.0258; open arm entries, p = 0.0550, unpaired t-test, n = 6–8 mice per group). **(C and C')** Depression-like behavior was assessed using forced swim test in PV Cre and PV Cre GluN2D$^{flox/flox}$ mice. PV Cre GluN2D$^{flox/flox}$ mice showed significantly higher mobility time as compared to PV Cre mice (*p = 0.0263, unpaired t-test) and significantly lower immobility time (*p = 0.0263, n = 8–9 mice per group). **(D)** In social interaction test, PV Cre GluN2D$^{flox/flox}$ mice showed significantly higher interaction time with stranger (animate) mouse (*p = 0.0469, unpaired t-test, n = 9 mice per genotype,). No significant change in time with inanimate object (p = 0.0991). **(E)** In novel object recognition task, PV Cre GluN2D$^{flox/flox}$ mice showed significantly less discrimination index in short-term memory test compared to the PV Cre mice (p = 0.0186, unpaired

t-test). No significant change in long-term memory test (p = 0.2605, unpaired t-test, n = 8–10 mice per group). **(F1)** Experimental timeline, briefly on day 0 mice were tested for side preference. On days 1–6, mice were trained for the habit acquisition and 7–12 days evaluated for the reversal learning. **(F2)** During habit acquisition PV Cre and PV Cre GluN2D$^{flox/flox}$ showed comparable learning with similar trials without errors (Two-way repeated measures ANOVA, genotype F (1, 156) = 0.0857, p=0.7701, n = 14 mice per genotype). **(F3)** The latency to reach the platform during the training phase was shorter in PV Cre GluN2D$^{flox/flox}$ (Two-way repeated measures ANOVA, genotype F (1, 156) = 14.54, p=0.0002). **(F4)** During reversal learning PV Cre GluN2D$^{flox/flox}$ mice showed significantly less number of trails without errors compared to the PV Cre mice (Two-way repeated measures ANOVA, genotype F (1, 26) = 9.982, p=0.0040, Bonferroni's post-hoc test revealed a significant difference in % trials without errors on day 1 ****p<0.0001 and day 2 ****p<0.0001. **(F5 and F6)** PV Cre GluN2D$^{flox/flox}$ mice showed significantly a greater number of perseverative errors (Two-way repeated measures ANOVA, genotype F (1, 26) = 7.488, p = 0.0110) and total errors (Two-way repeated measures ANOVA, genotype F (1, 156) = 9.997, p=0.0019) on day 1 and day 2 as compared to the PV Cre mice respectively. Bonferroni's post-hoc test revealed a significant difference in perseverative errors on day 1 and day 2 in PV Cre GluN2D$^{flox/flox}$ mice (day 1: **p = 0.0021; day 2: ***p = 0.008), as well as in total errors on day 1 and day 2 (day 1: **p = 0.0014; day 2: **p = 0.0039).

Table 1:

Electrophysiological, molecular networks and behavioral characteristics in PV-GluN2D KO mice supporting its modeling of schizophrenia.

Category	Schizophrenia (SZ) phenotype	PV-GluN2D KO phenotype	Relevance to Schizophrenia
Electrophysiology	Cortical Hyperexcitability	Higher sEPSCs in pyramidal neurons and PVIs.	✓
	Reduced inhibitory neurotransmission	Higher sIPSCs in pyramidal neurons but decrease in PVIs.	✗✓
Immunolabeling	Reduced PV labeling	Higher PV projections	✗
	GAD67 reduced	Reduced GAD67 labeling	✓
Molecular networks RNAseq: Transcriptomic, gene set enrichment and KEGG pathway	Alterations in Neurotransmitter Systems	GABAergic, Glutamatergic, and dopaminergic neurotransmitter systems were altered in PV-GluN2D KO mice.	✓
	GABAergic neurotransmission	GAD67, Slc32a1 or vGAT, Nlgn2, Cbln4 were downregulated and Gabra2 was upregulated	✓
	Glutamatergic neurotransmission	Increase in vGluT1 expression and downregulation of genes Cbln1, Nrg1 and ErbB4	✓
	Dopaminergic neurotransmission	Tyrosine hydroxylase (Th), dopamine transporter (Slc6a3), Dlx2 and Pax6 were downregulated	✓
	DEGs in Synaptogenesis	Mdga1, Agrn, Ptpro, Sv2c, Tenm3, Ntng1, Penk, Ap1s2 were downregulated	✓
	DEGs relevant to SZ	Btg, Cacng5, Chrm2, Ctxn3, Disc1, Dlx1, Fabp7, Grm4, Jag2, Kcna3, Mdga1, Mog, Nr4a2, Nrng1, Reln, Rgs12, and Vipr2 were downregulated	✓
	Calcium signaling	Calb2, Pde1c, Trdn, Adcy8, Cacna1s, Tacr1, Plcg2, and Chrm2 were downregulated	✓
Behavior	***Positive Symptoms***		
	Hyperlocomotion	Hyperlocomotion	✓
	Hypersensitivity to NMDA receptor channel blockers	Reduced or no change in sensitivity to MK-801-induced hyperlocomotion	✗
	Negative Symptoms		
	Depression-like behavior	Reduced depression-like behavior	✗
	Social deficits	Increase in social interaction	✗
	Cognitive Symptoms		
	Working memory deficits	Impaired cognitive behavioral flexibility, short-term memory deficit	✓
	Deficit in prepulse inhibition	No change in prepulse inhibition	✗
	Other behaviors		
	Anxiety-like behavior	Higher anxiety-like behavior	✓

KEY RESOURCES TABLE

Resource Type	Specific Reagent or Resource	Source or Reference	Identifiers	Additional Information
Add additional rows as needed for each resource type	Include species and sex when applicable.	Include name of manufacturer, company, repository, individual, or research lab. Include PMID or DOI for references; use “this paper” if new.	Include catalog numbers, stock numbers, database IDs or accession numbers, and/or RRIDs. RRIDs are highly encouraged; search for RRIDs at https://scicrunch.org/resources.	Include any additional information or notes if necessary.
Antibody	Rabbit polyclonal anti-Akt	Cell Signaling Technology	Cat # 9272, RRID: AB_329827	
	Rabbit polyclonal anti-PhosphoAkt^{Ser473}	Cell Signaling Technology	Cat # 9271, RRID: AB_329825	
	Rabbit polyclonal anti-calbindin	Santacruz Biotechnology	Cat # sc-28285; RRID: AB_2068334	
	Rabbit monoclonal anti-Cbln1	Abcam	Cat # ab1813779; RRID: AB_2480546	
	Rabbit polyclonal anti-Cbln4	Invitrogen	Cat # PA5-36472; RRID: AB_2850950	
	Mouse monoclonal anti-ErbB4	Invitrogen	Cat # MA5-13016, RRID: AB_10990351	
	Mouse monoclonal anti-Gabra2	Novus Biologicals	Cat # NBP2-59325; RRID: AB_2314469	
	Mouse monoclonal anti-Gad67	EMD Millipore	Cat # MAB5406, RRID: AB_2278725	
	Mouse monoclonal anti-Gapdh	EMD Millipore	Cat # MAB374, RRID: AB_2107445	
	Rabbit monoclonal anti- mTOR	Cell Signaling Technology	Cat # 2983, RRID: AB_2105622	
	Rabbit polyclonal anti-Phospho mTOR^{Ser2481}	Cell Signaling Technology	Cat # 2974, RRID: AB_2262884	
	Rabbit polyclonal anti-Neuregulin1	Proteintech	Cat # 10527-1-AP, RRID: AB_2154659	
	Mouse monoclonal anti-Neuroligin2	UC-Davis Neuromab	Cat # 75-451, RRID: AB_2651165	
	Mouse monoclonal anti-parvalbumin	Swant	Cat # PV235, RRID: AB_10000343	
	Rabbit anti-parvalbumin	Swant	Cat # PV27, RRID: AB_2631173	
	Rabbit anti-somatostatin	Peninsula Laboratories	Cat # T-4103, RRID: AB_518614	
	Mouse monoclonal anti-Tyrosine hydroxylase	Biolegend	Cat # 818002, RRID: AB_2564816	
	Guinea pig polyclonal anti-vGlut1	EMD Millipore	Cat # AB5905, RRID: AB_2301751	
	Chicken polyclonal anti-vGlut2	Synaptic systems	Cat # 135416, RRID: AB_2619824	
	Goat anti-rabbit conjugated to AlexaFluor 594	Thermo Fisher Scientific	Cat # A11012, RRID: AB_141359	
	Donkey anti-mouse conjugated to AlexaFluor 488	Thermo Fisher Scientific	Cat # A21202, RRID: AB_141607	
Chemical Compound or Drug	DQP-1105	Tocris Bioscience	Cat # 4491	
	Ro-25-6891	Alomone Labs	Cat # R-180	
	TCN201	Alomone Labs	Cat # T-190	

Resource Type	Specific Reagent or Resource	Source or Reference	Identifiers	Additional Information
Commercial Assay Or Kit	RNase Mini Kit	Qiagen	Cat # 74104	
	QIAshredder	Qiagen	Cat # 79654	
	Proteinase K	Qiagen	Cat # 19131	
Genetic Reagent	AAV5-EF1αa-DIO-mCherry	UNC vector core	-	
Organism/Strain	Grin2Dtm1a(EUCOMM)Wtsi	Wellcome Trust Sanger Institute	MGI:4432794	
	B6-SJL-Tg(ACTFLPe)9205Dym/J	Jackson Laboratories	Strain #:003800, RRID:IMSR_JAX:003800	
	PV-Cre mouse line	Jackson Laboratories	Strain #:017320, RRID:IMSR_JAX:017320	
Software; Algorithm	ANY-Maze	Stoelting Co.	https://www.any-maze.com/	
	BioRender	BioRender	https://biorender.com/	
	Graph Pad PRISM 7.0	GraphPad Software Inc.	https://www.graphpad.com/	
	iDEP.96	Ge et al., BMC Bioinformatics 2018 19, 534	http://bioinformatics.sdstate.edu/idep96/	
	ImageJ	NIH	https://imagej.nih.gov/ij/index.html	
	Metascape	Zhou et al. Nature Commun. 2019 10(1):1523	https://metascape.org/gp/index.html#/main/step1	
	ShinyGo	Ge et al., Bioinformatics 2020, 36:2628-2629	http://bioinformatics.sdstate.edu/go/	
	STRING	Szklarczyk et al., Nucleic acids research. 2019 47(D1): D607-13.	https://string-db.org/	
	SynGo	Koopman et al., Neuron 2019 103(2):217–234.e4.	https://www.syngoportal.org/	
	Topp Gene	Chen et al., 2009 37(Web Server issue): W305–11	https://toppgene.cchmc.org/enrichment.jsp	